Acoustic field mapping on GaAs using microscopic reflectance and reflectance anisotropy

Paulo V. Santos[a)]
Paul-Drude-Institut für Festkörperelektronik, Hausvogteiplatz 5-7, D-10117 Berlin, Germany

(Received 16 March 1999; accepted for publication 6 May 1999)

The mapping of surface acoustic wave (SAW) fields by means of microscopic reflectance and reflectance anisotropy in GaAs-based structures is reported. The two techniques are complementary with the second being sensitive to the strain and the first both to the strain and to the surface modulation induced by the SAW. Their combination provides information about both the longitudinal and transverse components of the SAW particle displacement vector. © *1999 American Institute of Physics.* [S0003-6951(99)04626-4]

The combination of surface acoustic waves (SAW) with GaAs technology opens new possibilities for high-frequency electro-optical devices.[1,2] Investigation of the piezoelectric fields, and of their interaction with carriers, requires techniques with high lateral (i.e., less than the SAW wavelength λ_{SAW}) and time (below the SAW period, $2\pi/\omega_{\mathrm{SAW}}$) resolution. Optical techniques are particularly convenient for these studies.[3,4] Although the lateral resolution of far-field optical measurements lies below that of scanning microscopy methods,[5] they are intrinsically fast and allow for spectroscopic probing of buried layers.

In this contribution, an optical scheme for the detection of piezoelectric SAW fields is presented based on microscopic measurements of the reflectance changes (ΔR_{SAW}) and of the reflectance polarization anisotropy (δR_{SAW}) induced by a SAW with a diffraction-limited lateral resolution of 1–2 μm. For photon energies away from electronic resonances, it is demonstrated that δR_{SAW} is determined by the elasto-optic modulation of the optical properties by the SAW strain, while ΔR_{SAW} depends both on the strain and on the surface modulation induced by the SAW. The two techniques thus provide complementary information about the longitudinal and transverse components of the SAW displacement vector.

The experimental setup, illustrated schematically in Fig. 1, achieves response frequencies up to about 1 GHz without requiring pulsed lasers. The laser source is chopped (C), spatially filtered (SP), and focused to a 2 μm (1 μm) spot on the sample surface by a 50× (100×) objective (O) lense. Radiation from a continuous, frequency-doubled Nd–vanadate ($Nd:YVO_4$) laser ($\lambda_L = 532$ nm) was employed with an intensity <0.4 mW on the sample surface. The reflected light is collected by the same objective and detected by a fast pin photodiode (PD, Hamamatsu 5973, active area diameter of 400 μm). Due to the modulation of the optical properties by the SAW, the detected reflection intensity R depends on the spot position x' on the sample surface according to

$$R = R_0 + \Delta R_{\mathrm{SAW}} \cos(k_{\mathrm{SAW}} x' - \omega_{\mathrm{SAW}} t), \tag{1}$$

where $k_{\mathrm{SAW}} = 2\pi/\lambda_{\mathrm{SAW}}$ and $\mathbf{x}' \| \mathbf{k}_{\mathrm{SAW}}$. R_0 and ΔR_{SAW} denote, respectively, the average and the SAW-induced effective reflectivities detected by the PD. As will be discussed in detail below, ΔR_{SAW} contains contributions from the dielectric constant modulation and from the surface topography modulation induced by the SAW. A lock-in amplifier is employed to detect the component of the PD signal with the chopper frequency V_c, which is used to monitor R_0. The high-frequency components are amplified and mixed with ω_{SAW}. The mixing yields a signal V_{rf} at the chopper frequency, which is detected by a second lock-in amplifier. V_{rf} is proportional to ΔR_{SAW} according to

$$\frac{V_{\mathrm{rf}}}{V_c} = A \frac{\Delta R_{\mathrm{SAW}}}{R_0} \cos(k_{\mathrm{SAW}} x'), \tag{2}$$

where A is the effective gain of the amplifying and mixing stages.

The anisotropy was measured by including a photoelastic modulator (PEM) and polarizers (P and A) in the optical path of Fig. 1. The arrangement of the optical components is the same as that employed for measurements of static (i.e., time-independent) anisotropies in Ref. 6. For the detection of the time-dependent SAW-induced anisotropy, the signal V_{2M}

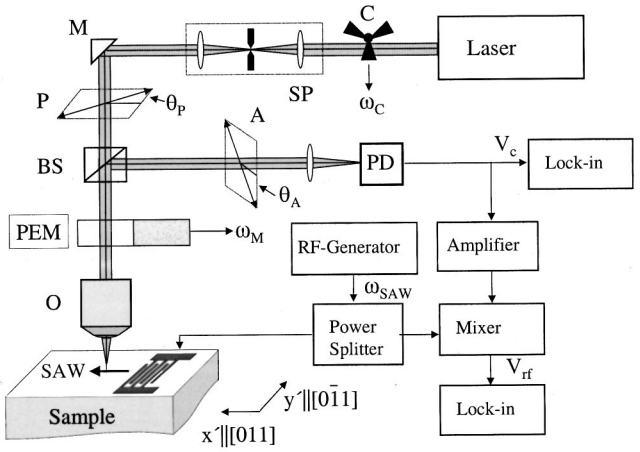

FIG. 1. Experimental setup for microscopic optical measurements: A: analyzer, BS: beam splitter, C: chopper, M: mirror, O: objective lens, P: polarizer, PD: photodiode, PEM: photoelastic modulator, and SP: spatial filter. For the anisotropy measurements, θ_P and θ_A were aligned along the optical axes $x'+y'$ and y', respectively, with $x' = [011]$ and $y' = [0\bar{1}1]$.

[a)]Corresponding author: Electronic mail: santos@pdi-berlin.de.

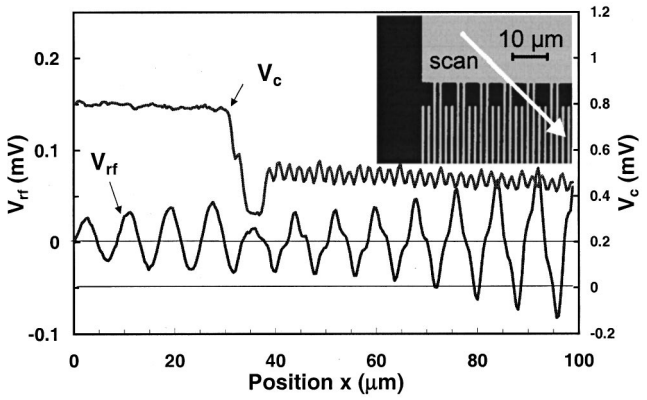

FIG. 2. Profiles of V_c (right scale) and of $V_{\rm rf}$ (left scale) for sample B, recorded simultaneously while scanning the laser spot across the section of the IDT indicated in the inset. V_c and $V_{\rm rf}$ correspond, respectively, to the average reflection and to the reflection changes induced by the SAW.

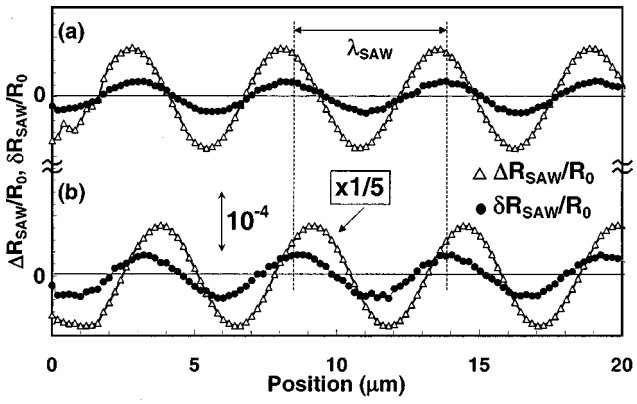

FIG. 3. SAW-induced reflectance ($\Delta R_{\rm SAW}/R_0$, triangles) and reflectance anisotropy ($\delta R_{\rm SAW}/R_0$, circles) of sample A recorded simultaneously in front of the IDT (see the inset of Fig. 2) (a) without and (b) with a stop (a knife edge) introduced after the analyzer in Fig. 1 to partially block the reflected beam.

at the mixer output at twice the modulator frequency ω_M was detected using a lock-in amplifier. The anisotropy is then given by $\delta R_{\rm SAW}/R_0 = 2(R_{x'} - R_{y'})/(R_{x'} + R_{y'}) = [A/J_2(\chi_0)]V_{2M}/V_c$, where $R_{x'}$ ($R_{y'}$) is the reflectance for polarization along the surface direction $\mathbf{x}' \| \mathbf{k}_{\rm SAW}$ ($\mathbf{y}' \perp \mathbf{k}_{\rm SAW}$). The Bessel function J_2 assumes a value $J_2(\chi_0) = 0.43$ for a PEM retardation of $\chi_0 = 2.404$ rad at λ_L.

The measurements reported here were performed on a (100) GaAs substrate (sample A) and on a (100) GaAs(3 nm)/$Al_{0.3}Ga_{0.7}As$(300 nm)/GaAs layered structure grown by molecular beam epitaxy (sample B). For both samples, the penetration depth of the $\lambda_L = 532$ nm radiation is less than 20 nm, so that only the top layers are probed. SAW propagating along the $x' \| [011]$ direction were generated by split-finger interdigital transducers (IDTs). The IDTs were designed for operation at $\lambda_{\rm SAW} = 5.6\,\mu$m (corresponding to central frequencies of $\omega_{\rm SAW} = 511$ MHz and $\omega_{\rm SAW} = 515$ MHz for samples A and B, respectively). They consist of 700 pairs of $0.7 \times 120\,\mu m^2$ aluminum fingers with a center-to-center distance of 1.4 μm. All measurements were performed at room temperature with a rf excitation power of 13 dBm applied to the IDT. Due to electrical mismatching, the acoustic power is 5.2 dB lower, as determined by rf reflection.

Figure 2 displays profiles of the components of V_c and $V_{\rm rf}$ in phase with the chopper transmission, obtained while scanning the laser spot across the IDT along the line indicated in the inset. The two signals were recorded simultaneously in a single scan to ensure that they correspond to the same position on the sample surface. Because of the high Al reflection, V_c achieves its maximum in the contact pad area ($0 < x < 28\,\mu$m), decreases to the semiconductor reflection levels for $34 < x < 36\,\mu$m, and exhibits oscillations in the finger region ($x > 36\,\mu$m). These oscillations have a period corresponding to the center-to-center distance between the Al fingers of $1.4\sqrt{2}\,\mu$m, where the $\sqrt{2}$ factor accounts for the oblique scan direction. The signal $V_{\rm rf}$ displays oscillations with a period of $\sqrt{2}\lambda_{\rm SAW}$. In the finger area, their sinusoidal shape is deformed by the metal fingers. The oscillations in Fig. 2 are attributed to the SAW-induced changes in reflectance, $\Delta R_{\rm SAW}$. This conclusion is corroborated by the fact that they are suppressed when the rf is detuned with respect to the IDT resonance band. The oscillation amplitude on the contact pad decreases with x since the SAW becomes evanescent.

Figure 3(a) compares profiles for $\Delta R_{\rm SAW}/R_0$ and $\delta R_{\rm SAW}/R_0$ for sample A, recorded simultaneously while scanning the laser spot along the SAW propagation direction in front of the IDT. For these measurements, the focus on the sample and the position of the reflection spot on the PD were adjusted so as to maximize V_c. The anisotropy signal, of the order of 5×10^{-5}, is smaller and almost in phase with respect to $\Delta R_{\rm SAW}/R_0$.

In order to investigate the reflection modulation mechanisms, we first note that as for $\Delta R_{\rm SAW}/R_0$, the anisotropy $\delta R_{\rm SAW}/R_0$ is strongly reduced under the metal and vanishes when the driving rf is detuned. Measurements within the transducer showed that both $\Delta R_{\rm SAW}/R_0$ and $\delta R_{\rm SAW}/R_0$ are suppressed under detuned excitation. Since an electric (but no acoustic) field is still present under these conditions, we conclude that the mechanism responsible for the reflectance modulation is of elasto-optic (rather than electro-optic[7]) nature.

The longitudinal (u_x) and transverse (u_z) displacement fields of a Rayleigh SAW can be written as[8,9]

$$u_{x'}(x',z,t) = u_{x'0}(z)e^{i(k_{\rm SAW}x' - \omega_{\rm SAW}t)}, \tag{3}$$

$$u_z(x',z,t) = iu_{z0}(z)e^{i(k_{\rm SAW}x' - \omega_{\rm SAW}t)}, \tag{4}$$

where $u_{x'0}(z)$ and $u_{z0}(z)$ are real functions. Two mechanisms may contribute to the modulation $\Delta R_{\rm SAW}$. The first is associated with the modulation of the dielectric tensor $\boldsymbol{\epsilon}$ by the strain accompanying the SAW (photoelastic effect). For a Rayleigh SAW on an isotropic or cubic material, the SAW-induced changes in $\boldsymbol{\epsilon}$, $\Delta\boldsymbol{\epsilon}_{\rm SAW}$, can be expressed in the basis $\{x' \| [011], y' \| [0\bar{1}1]\}$ as

$$\Delta\boldsymbol{\epsilon}_{\rm SAW} = \Delta\epsilon_{\rm iso}\begin{bmatrix}1 & 0\\ 0 & 1\end{bmatrix} + \frac{\Delta\epsilon_{\rm ani}}{2}\begin{bmatrix}1 & 0\\ 0 & -1\end{bmatrix}. \tag{5}$$

Here, $\Delta\epsilon_{\rm iso} = [(p_{11}+p_{12})/2u_{x'x'} + p_{12}u_{zz}]$, and $\Delta\epsilon_{\rm ani} = 2[(p_{11}-p_{12})/2u_{x'x'}]$, where the $p's$ are the photoelastic coefficients relating the changes in $\boldsymbol{\epsilon}$ to the strains $u_{x'x'} = \partial u_{x'}/\partial x'$ and $u_{zz} = \partial u_z/\partial z$. The first contribution in Eq. (5) is isotropic and associated with the local volume change

induced by the SAW strain. It leads to intensity fluctuations and to angular deflections of the reflected beam (see below). The second contribution, related to $\Delta\epsilon_{\mathrm{ani}}$, arises from the symmetry reduction induced by the strain. It leads to different optical responses for light polarization along and perpendicular to the SAW wave fronts. The anisotropy induced by $\Delta\epsilon_{\mathrm{ani}}$ accounts for the anisotropy $\delta R_{\mathrm{SAW}}/R_0$ displayed in Fig. 3(a): it depends only on the longitudinal displacement through $u_{x'x'}$ and oscillates with frequency ω_{SAW}.

The strain-induced reflectance modulation can be estimated using the measured values for the elasto-optical coefficients of GaAs.[10] For this purpose, the strains will be assumed constant within the short light penetration depth ($\ll\lambda_{\mathrm{SAW}}$) and equal to the value at the surface. In addition, we neglect the effects associated with the finite lateral resolution and with the presence of surface overlayers on the reflection. Under these conditions, the modulation in ϵ leads to reflectance and reflectance anisotropy modulations given by $\Delta R_{\mathrm{SAW}}/R_0 = 2\,\mathrm{Re}[g\Delta\epsilon_{\mathrm{iso}}]$ and $\delta R_{\mathrm{SAW}}/R_0 = 2\,\mathrm{Re}[g\Delta\epsilon_{\mathrm{ani}}]$, respectively, with $g=(\epsilon-1)/\epsilon^{3/2}$. The strains were determined following the procedure outlined in Ref. 9. The calculations yield rms values $\Delta R_{\mathrm{SAW}}/R_0 \sim 10^{-4}$ and $\delta R_{\mathrm{SAW}}/R_0 \sim 10^{-5}$ for the applied acoustic power. These values are comparable to the amplitudes measured in Fig. 3(a).

The second mechanism for the SAW-induced modulation of the PD current is associated with angular deflections of the laser beam upon reflection on the sample. Such deflections may be introduced by the modulation of the surface slope $\alpha(x,t)=\partial u_z/\partial x'$ induced by the SAW or by lateral gradients of the dielectric function induced by the strain. Beam deflections due to surface modulation have been extensively studied in the SAW literature,[3,11] where they have been successfully used for probing acoustic fields. The deflections also yield a contribution to the anisotropy. This contribution, however, oscillates at $2\omega_{\mathrm{SAW}}$ and can thus be easily distinguished from that associated with the $\Delta\epsilon_{\mathrm{ani}}$, which oscillates at ω_{SAW}.

Beam deflection modulations of ΔR_{SAW} can be minimized by careful alignment of the optical components in the setup of Fig. 1. Their influence is demonstrated in Fig. 3(b). Here, the profiles were recorded under the same conditions as in Fig. 3(a), except that a stop (a knife edge[3,11]) was introduced in the laser path just after the analyzer, so as to partially block the reflected beam. The asymmetry introduced by the knife edge makes the PD current different for positive and negative surface angles α. The amplitude of $\Delta R_{\mathrm{SAW}}/R_0$ is enhanced by a factor of 5 and its phase shifts by about 90°. The phase shift is consistent with the fact that the maxima of α are dephased by 90° with respect to those of u_z. Note that the changes in $\delta R_{\mathrm{SAW}}/R_0$ are much less pronounced than those in $\Delta R_{\mathrm{SAW}}/R_0$, in agreement with the previous discussion.

In conclusion, a simple procedure was presented for the optical probing of high-frequency SAW fields in GaAs-based structures based on microscopic reflectance and reflectance anisotropy measurements. For photon energies away from electronic resonances, the two techniques deliver complementary information about the acoustic displacement field: the SAW-induced reflection anisotropy depends only on the longitudinal component of the displacement field, while the reflection modulation has contributions from both the longitudinal and transversal components.

The author thanks E. Chilla, C. Flannery, H. Grahn, and R. Koch for helpful discussions and W. Seidel and S. Krauß for the fabrication of the SAW structures.

[1] M. J. Hoskins, H. Morkoç, and B. J. Hunsinger, Appl. Phys. Lett. **41**, 332 (1982).
[2] C. Rocke, S. Zimmermann, A. Wixforth, J. P. Kotthaus, G. Böhm, and G. Weimann, Phys. Rev. Lett. **78**, 4099 (1997).
[3] H. Sontag and A. C. Tam, IEEE Trans. Ultrason. Ferroelectr. Freq. Control **UFFC-33**, 500 (1986).
[4] P. V. Santos, M. Ramsteiner, and F. Jungnickel, Appl. Phys. Lett. **72**, 2099 (1998).
[5] T. Hesjedal, E. Chilla, and H.-J. Fröhlich, Appl. Phys. Lett. **69**, 354 (1996).
[6] B. Koopmans, B. Richards, P. Santos, K. Eberl, and M. Cardona, Appl. Phys. Lett. **69**, 782 (1996).
[7] R. E. Chang, S. M. Richie, K. J. Casey, and D. C. Malocha, in *1993 IEEE Ultrason. Symp. Proceedings*, edited by M. Levy and B. R. McAvoy (Institute of Electrical and Electronic Engineers, New York, 1993), p. 227.
[8] R. Stoneley, Proc. R. Soc. London, Ser. A **232**, 447 (1955).
[9] S. Simon, Phys. Rev. B **54**, 13878 (1996).
[10] P. Etchegoin, J. Kircher, M. Cardona, C. Grein, and E. Bustarret, Phys. Rev. B **46**, 15139 (1992).
[11] L. Whitman and A. Korpel, Appl. Opt. **8**, 1567 (1969).